

Purine but Not Pyrimidine Nucleotides Support Rotation of F_1 -ATPase*

Received for publication, March 12, 2001, and in revised form, March 28, 2001
Published, JBC Papers in Press, March 28, 2001, DOI 10.1074/jbc.M102200200

Hiroyuki Noji^{‡§}, Dirk Bald^{¶¶}, Ryohei Yasuda^{‡||}, Hiroyasu Itoh^{‡**}, Masasuke Yoshida^{‡‡‡}, and Kazuhiko Kinoshita, Jr.^{‡§§¶¶}

From [‡]CREST “Genetic Programming” Team 13, Teikyo University Biotechnology Research Center 3F, Nogawa 907, Miyamae-ku, Kawasaki 216-0001, Japan, [§]PRESTO, Chemical Resources Laboratory, Tokyo Institute of Technology, Yokohama 226-8503, Japan, ^{**}Tsukuba Research Laboratory, Hamamatsu Photonics KK, Tokodai, Tsukuba 300-2635, Japan, ^{‡‡}Chemical Resources Laboratory, Tokyo Institute of Technology, Yokohama 226-8503, Japan, and ^{§§}Faculty of Science and Technology, Keio University, Yokohama 223-8522, Japan

The binding change model for the F_1 -ATPase predicts that its rotation is intimately correlated with the changes in the affinities of the three catalytic sites for nucleotides. If so, subtle differences in the nucleotide structure may have pronounced effects on rotation. Here we show by single-molecule imaging that purine nucleotides ATP, GTP, and ITP support rotation but pyrimidine nucleotides UTP and CTP do not, suggesting that the extra ring in purine is indispensable for proper operation of this molecular motor. Although the three purine nucleotides were bound to the enzyme at different rates, all showed similar rotational characteristics: counterclockwise rotation, 120° steps each driven by hydrolysis of one nucleotide molecule, occasional back steps, rotary torque of ~40 piconewtons (pN)·nm, and mechanical work done in a step of ~80 pN·nm. These latter characteristics are likely to be determined by the rotational mechanism built in the protein structure, which purine nucleotides can energize. With ATP and GTP, rotation was observed even when the free energy of hydrolysis was -80 pN·nm/molecule, indicating ~100% efficiency. Reconstituted F_0F_1 -ATPase actively translocated protons by hydrolyzing ATP, GTP, and ITP, but CTP and UTP were not even hydrolyzed. Isolated F_1 very slowly hydrolyzed UTP (but not CTP), suggesting possible uncoupling from rotation.

The F_0F_1 ATP synthase is an enzyme that synthesizes ATP from ADP and inorganic phosphate (P_i) using proton flow across a membrane (1). The F_0 portion of the enzyme resides in the membrane and mediates proton translocation. The F_1 portion, consisting of $\alpha_3\beta_3\gamma_1\delta_1\epsilon_1$ subunits, is external to the membrane and catalyzes ATP synthesis. The ATP synthase is a completely reversible molecular machine in that ATP hydrolysis in F_1 can produce a reverse flow of protons through F_0 . Isolated F_1 only catalyzes ATP hydrolysis and hence is called F_1 -ATPase. Its minimal, stable subcomplex capable of ATP hydrolysis is $\alpha_3\beta_3\gamma$ (2).

For the coupling between the proton flow in F_0 and the

chemical reaction (ATP synthesis/hydrolysis) in F_1 , Boyer and Kohlbrenner (3) and Oosawa and Hayashi (4) independently suggested a rotational catalysis model. The essence is that F_0 is a rotary motor (or turbine) driven by the proton flow, that F_1 is another rotary motor driven by ATP hydrolysis, and that the two motors have a common rotary shaft, yet their genuine rotary directions are opposite to each other's. Rotation of the shaft in F_0 's genuine direction, as occurs in cells, results in the reverse rotation of the F_1 motor and thus in ATP synthesis in F_1 . When F_1 gains control and hydrolyzes ATP, protons are pumped through F_0 in the reverse direction.

A crystal structure of F_1 (5) strongly supported the rotation model and has inspired many experiments, which, together, have proved that the γ subunit is (part of) the common rotor shaft and that $\alpha_3\beta_3$ subunits, which surrounded γ in the crystal, are the stator in the F_1 motor (6–8). Single-molecule imaging of F_1 , in particular, has revealed that the γ subunit rotates in a unique direction consistent with the crystal structure, that γ makes discrete 120° steps, and that the energy conversion efficiency of the F_1 motor driven by ATP hydrolysis can reach ~100% (9, 10). The precise mechanism of rotation, however, is not yet clear.

In Boyer's model, binding changes play the major role (1). On the three β subunits, each of which hosts a catalytic site, ATP and its hydrolysis products, ADP and P_i , are in equilibrium. Thus, in the absence of an external energy supply, the change in free energy associated with ATP hydrolysis should manifest as the higher affinity for ATP than for ADP and P_i . During ATP synthesis, the mechanical energy supplied by the γ rotation driven by F_0 somehow decreases the affinity for ATP (and probably increases the affinity for ADP and P_i), resulting in the appearance of ATP in the medium. In the reverse reaction of ATP hydrolysis, the free energy difference between the stronger ATP binding and weaker ADP/ P_i binding drives the rotation of γ . Boyer proposes that these binding changes occur sequentially on the three catalytic sites, synchronously with the γ rotation. In the crystal structure of F_1 (5), the three β subunits carried a different nucleotide, an analog of ATP, ADP, and none, in support of the sequential binding change mechanism.

If binding and release, rather than the cleavage of the terminal phosphate, are indeed the source of mechanical torque production in the F_1 motor, the rotational characteristics are expected to differ among different NTPs. The free energy gain in overall hydrolysis is similar among NTPs, but the operation of the F_1 motor, which can work at near 100% efficiency, may well depend on delicate energy balances in various steps of hydrolysis. Here we show that purine but not pyrimidine nu-

* The costs of publication of this article were defrayed in part by the payment of page charges. This article must therefore be hereby marked “advertisement” in accordance with 18 U.S.C. Section 1734 solely to indicate this fact.

^{¶¶} Present address: Dept. of Structural Biology, Free University of Amsterdam, De Boelelaan 1087, 1081, Amsterdam, Netherlands.

^{||} Present address: Cold Spring Harbor Laboratory, 1 Bungtwon Rd., Cold Spring Harbor, NY 11724.

^{¶¶¶} To whom correspondence should be addressed. Tel.: 81 44 750 1710; Fax: 81 44 750 1712.

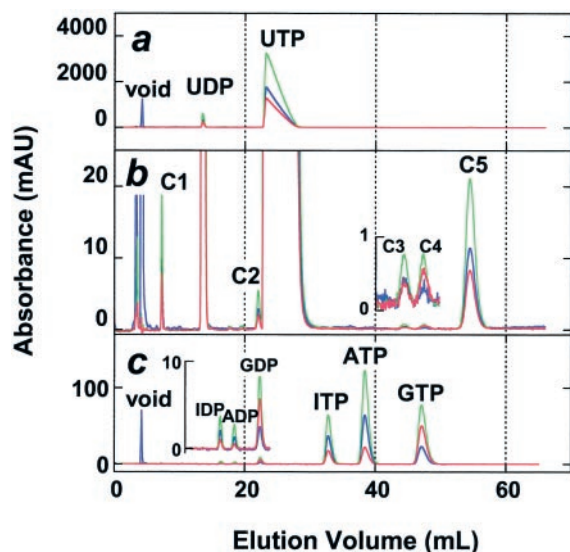


FIG. 1. **Contaminants in UTP.** 775 nmol of UTP was loaded on the anion exchange column equilibrated with 50 mM sodium phosphate (pH 7.0) and eluted with an isocratic flow of the equilibration buffer. *a*, elution profiles monitored as A_{220} (blue), A_{260} (green), and A_{280} (red). UTP contained UDP at 3%. *b*, expansions of profiles in *a*. *Inset*, further expansion. Five contaminant peaks, C1–C5, were resolved. *c*, elution profiles for combined purine nucleotides. 20 nmol of ATP, 10 nmol of GTP, and 10 nmol of ITP were loaded together. *Inset*, their expanded profiles. Contaminating ADP, GDP, and IDP were eluted before ATP, GTP, and ITP. Peak C4 was identified as GTP from the coincidence in the elution time and the relative magnitudes of A_{220} , A_{260} , and A_{280} . The amounts of the contaminants in C1–C5 were 0.10, 0.03, 0.01, 0.01, and 0.39% of UTP, respectively.

cleotides support F_1 rotation, suggesting that the interaction between the catalytic site and the additional ring in purines is critical to the proper operation of this molecular machine.

EXPERIMENTAL PROCEDURES

Chemicals and Proteins—Nucleotides (GTP, ITP, UTP, and CTP) were purchased from Sigma. ATP and other enzymes were from Roche Molecular Biochemicals. The purity of each nucleotide was assessed on an anion exchange column. Nucleotides were applied on DEAE 2SW (Tosoh, Japan) equilibrated with 50 mM sodium phosphate (pH 7.0) and eluted with an isocratic flow of the same buffer. Because DEAE 2SW has higher affinity for compounds with more negative charges, nucleotides are eluted in the order of nucleoside mono-, di-, and triphosphate. The elution profiles for UTP are shown in Fig. 1, *a* and *b*. Besides the UDP peak at 13 ml (identical with the peak for commercial UDP), several contaminant peaks (C1–C5) were resolved. The void peak at 4 ml is unlikely to be a nucleotide(s), because A_{260} (green) and A_{280} (red), within an absorbance peak of a nucleotide, were extremely low compared with A_{220} (blue). C1 at 7 ml was probably UMP, because it was eluted earlier, and the relative magnitudes of A_{220} , A_{260} and A_{280} were the same as those for UTP and UDP. C4 was judged as contaminating GTP, because its elution volume and the relative magnitudes of A_{220} , A_{260} , and A_{280} all matched with those for GTP (Fig. 1c). The GTP contamination amounted to 0.01% of UTP, as determined from the peak area of A_{260} . The other contaminants, C2, C3, and C5, were of unknown origin; their signatures did not match with those of ATP, GTP, ITP, dATP, or their diphosphates. C2, C3, and C5 in UTP amounted to 0.03, 0.01, and 0.39%, respectively. Although the levels of contaminants were low, they may nevertheless affect the rotation assay, because the affinity of F_1 -ATPase for UTP is extremely low (see “Results”). We therefore used the fraction at the UTP peak (23 ml) for the rotation assay. CTP was also found to be contaminated by unknown compounds (1.5%); thus, its peak fraction was used for the rotation assay. ATP, GTP, and ITP contained less than 5% contaminants, which were mostly their hydrolysis products; these were used without purification.

The $\alpha_3\beta_3\gamma$ subcomplex (β -His tag/ γ S107C) of F_1 derived from thermophilic *Bacillus* strain PS3 (TF₁)¹ was expressed in *Escherichia coli*

as described previously (9) and purified as follows. The cell lysate containing the enzyme was applied on a Ni²⁺-NTA Superflow column (Qiagen) equilibrated with 50 mM imidazole (pH 7.0) and 100 mM NaCl. The column was washed with 100 mM imidazole (pH 7.0) and 100 mM NaCl, and then the enzyme was eluted with 500 mM imidazole (pH 7.0) and 100 mM NaCl. Ammonium sulfate was added to the fraction containing the enzyme to a final concentration of 10% saturation and the sample was applied to a butyl-Toyopearl column (Tosoh, Japan) equilibrated with 500 mM imidazole (pH 7.0), 100 mM NaCl, and 10% saturated ammonium sulfate. The column was washed with 10 column volumes of a solution containing 100 mM sodium phosphate (pH 7.0), 2 mM EDTA, and 10% saturated ammonium sulfate to remove endogenously bound nucleotides. The enzyme was eluted with 50 mM Tris-Cl (pH 8.0) and 2 mM EDTA and stored as precipitant in 70% saturated ammonium sulfate containing 2 mM dithiothreitol. Before use, the enzyme was dissolved in 100 mM sodium phosphate (pH 7.0) and 2 mM EDTA and passed through a size exclusion column (Superdex 200 HR 10/30; Amersham Pharmacia Biotech) equilibrated with 100 mM sodium phosphate (pH 7.0) and 2 mM EDTA. The amount of nucleotides remaining on the enzyme was determined as described previously (11). Samples with less than 0.1 mol of nucleotide/mol of enzyme were used for the measurement of hydrolysis activity. Whole TF₁F_o complex was reconstituted from the mutant TF₁ (β -His tag/ γ S107C) and authentic F_o from the thermophile and was incorporated into liposomes as described previously (12).

NTPase Activity—ATP, GTP, ITP, and UTP hydrolysis activities of $\alpha_3\beta_3\gamma$ were measured at 23 °C in a medium containing 50 mM MOPS-KOH (pH 7.0), 50 mM KCl, 2 mM MgCl₂, and an ATP (or GTP, ITP, or UTP)-regenerating system consisting of 2.5 mM phosphoenolpyruvate, 100 μ g/ml lactate dehydrogenase, 0.2 mM NADH, and pyruvate kinase at 200 μ g/ml for ATP hydrolysis, 500 μ g/ml for GTP and ITP hydrolysis, or 750 μ g/ml for UTP hydrolysis. The reaction was initiated by the addition of the enzyme to 1.3 ml of assay mixture, and hydrolysis was monitored as NADH oxidation determined from the absorbance decrease at 340 nm. The CTP hydrolysis activity was estimated from P_i released in the same medium without a regenerating system during a 60-min incubation at 23 °C. Hydrolysis by the reconstituted TF₁F_o was also measured as P_i released in 50 mM MOPS-KOH (pH 7.0), 25 mM Na₂SO₄, 25 mM K₂SO₄, 4 mM MgCl₂, and 2 mM indicated nucleotide during a 20-min incubation at 23 °C.

Rotation Assay—Streptavidin-conjugated TF₁ for the rotation assay was prepared as described previously (9). Rotation in the presence of ATP, GTP, or ITP was observed in the TF₁ adsorbed on a Ni²⁺-NTA-modified polystyrene bead by attaching an actin filament to the γ subunit (10). The assay mixture contained 50 mM MOPS-KOH, (pH 7.0), 50 mM KCl, 2 mM MgCl₂, 10 mg/ml bovine serum albumin, and an indicated Mg-nucleotide. Fluorescent actin filaments at the bottom of a flow chamber were observed with an inverted epifluorescence microscope (IX70; Olympus). Assays at less than 10 μ M GTP or ITP were made on the TF₁ directly attached to coverslips to which Ni²⁺-NTA had been bound covalently (13); the probability of finding a rotating actin filament was higher than on the Ni²⁺-NTA-modified polystyrene bead. Images were taken with an intensified CCD camera (ICCD-350F; VideoScope) and recorded on 8-mm videotapes. Rotation by UTP or CTP was observed through an aggregate of biotinylated polystyrene beads with a diameter of 440 nm, which was attached to γ (14). Images of bead aggregates were obtained in the bright field in the absence of the oxygen scavenger system and recorded with a CCD camera (CCD-300-RC; Dage-MTI). Possible nucleotide contamination from actin filaments and the oxygen scavenger system was thus excluded.

Proton Pump by Reconstituted TF₁F_o—Nucleotide-driven proton-translocation into TF₁F_o liposomes was detected as the decrease in the pyranine fluorescence in an FP 777 fluorometer (JASCO, Japan) at 23 °C. TF₁F_o liposomes (about 5 μ g of TF₁F_o) containing pyranine inside were preincubated at 23 °C in 1.5 ml of a reaction mixture containing 10 mM MOPS-KOH (pH 7.0), 50 mM KCl, 2 mM nucleotide, 25 mM K₂SO₄, 25 mM Na₂SO₄, and 20 mM *p*-xylene-bispyridinium bromide, which quenched the pyranine fluorescence outside the liposomes. Excitation and emission wavelengths were 460 and 510 nm, respectively. The reaction was started by the addition of 4 mM MgCl₂. After recording the fluorescence change, 10 μ M FCCP was added to recover the initial fluorescence, which would ensure that the fluorescence decrease was caused by the proton uptake into the liposomes.

¹ The abbreviations used are: TF₁, the $\alpha_3\beta_3\gamma$ subcomplex (β -His tag/ γ S107C) of F_1 derived from thermophilic *Bacillus* strain PS3; NTA, nitrilo-

triacetic acid; FCCP, carbonyl cyanide *p*-(trifluoromethoxy) phenylhydrazone; TF₁F_o, F₁F_o-ATPase derived from thermophilic *Bacillus* strain PS3; MOPS, 4-morpholinepropanesulfonic acid; pN, piconewton(s).

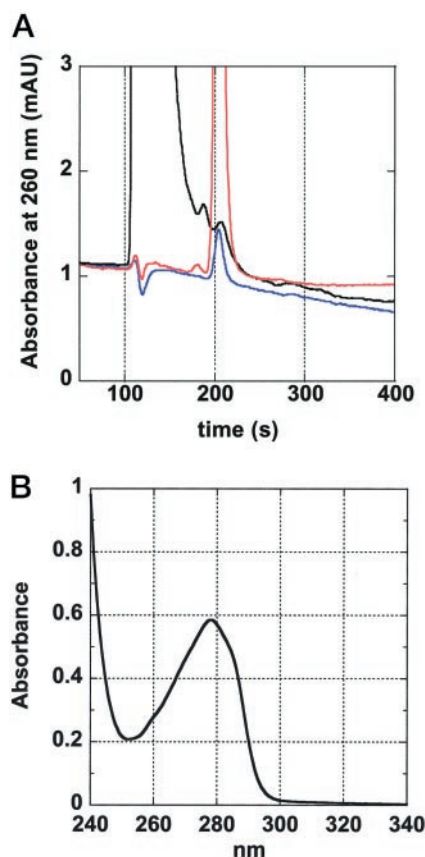


FIG. 2. **Nucleotide-depleted $\alpha_3\beta_3\gamma$ subcomplex.** *a*, assessment of nucleotides tightly bound to the $\alpha_3\beta_3\gamma$ subcomplex. 100 pmol of the purified subcomplex was precipitated by perchloric acid and subjected to reverse-phase chromatography with the monitor wavelength of 260 nm (black line). Bound ATP and ADP gave peaks at 188 and 208 s, respectively, with a height of 0.49 and 0.23 milliabsorbance units above the tail of the main peak. As controls, 10 pmol of ADP gave a peak at 204 s with a height of 1.28 milliabsorbance units (blue line), and 100 pmol of the commercial ADP showed a contaminant ATP peak at 183 s (red line). *b*, absorbance spectrum of the nucleotide-depleted $\alpha_3\beta_3\gamma$ subcomplex. The ratio of A_{280} (0.57) to A_{260} (0.279) was 2.04.

RESULTS

Nucleotide-depleted F_1 -ATPase— F_1 -ATPase is known to be inhibited by Mg-ADP tightly bound to a catalytic site (15, 16). TF_1 used in the previous study (10) contained ~ 0.3 mol of tightly bound nucleotide/mol of enzyme; thus, the hydrolysis activity might have been underestimated. Here, we employed an improved purification protocol (see “Experimental Procedures”) and obtained a sample containing only 0.084 mol of bound nucleotide (0.037 mol of ATP and 0.047 mol of ADP) per mol of enzyme as determined from the peak heights in the reverse-phase chromatography (Fig. 2*a*). Before use, the protein was further purified by size exclusion chromatography, because TF_1 tended to aggregate upon storage. For the final sample, the ratio of A_{280} to A_{260} , a convenient measure of the purity, was greater than 2.0 (Fig. 2*b*). As expected, the ATP hydrolysis activity of this nucleotide-depleted enzyme was higher than that reported previously (see below).

Hydrolysis Activities—ATP, GTP, ITP, and UTP hydrolysis activities of the nucleotide-depleted TF_1 were determined as the rate of oxidation of NADH using the ATP-, GTP-, ITP-, or UTP-regenerating system. Hydrolysis of the purine nucleotides, ATP, GTP, and ITP, gradually decelerated to a steady state as shown in Fig. 3, *a* and *b*. This turnover-dependent inactivation is attributed to the Mg-ADP (GDP, IDP) inhibition. The hydrolysis rates were therefore determined during the initial 10 s after the injection of the enzyme into the assay

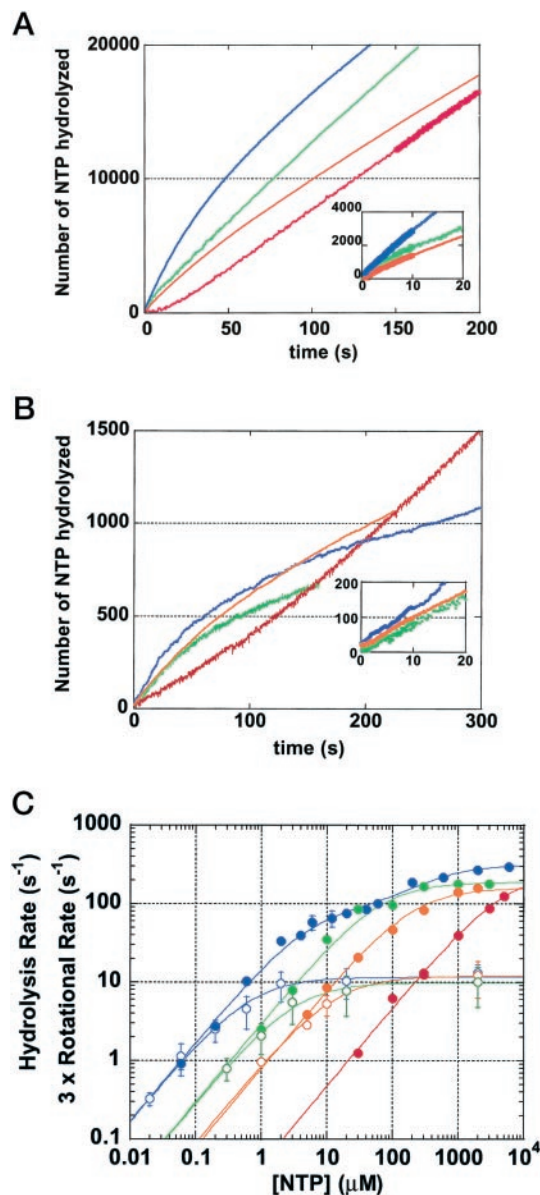
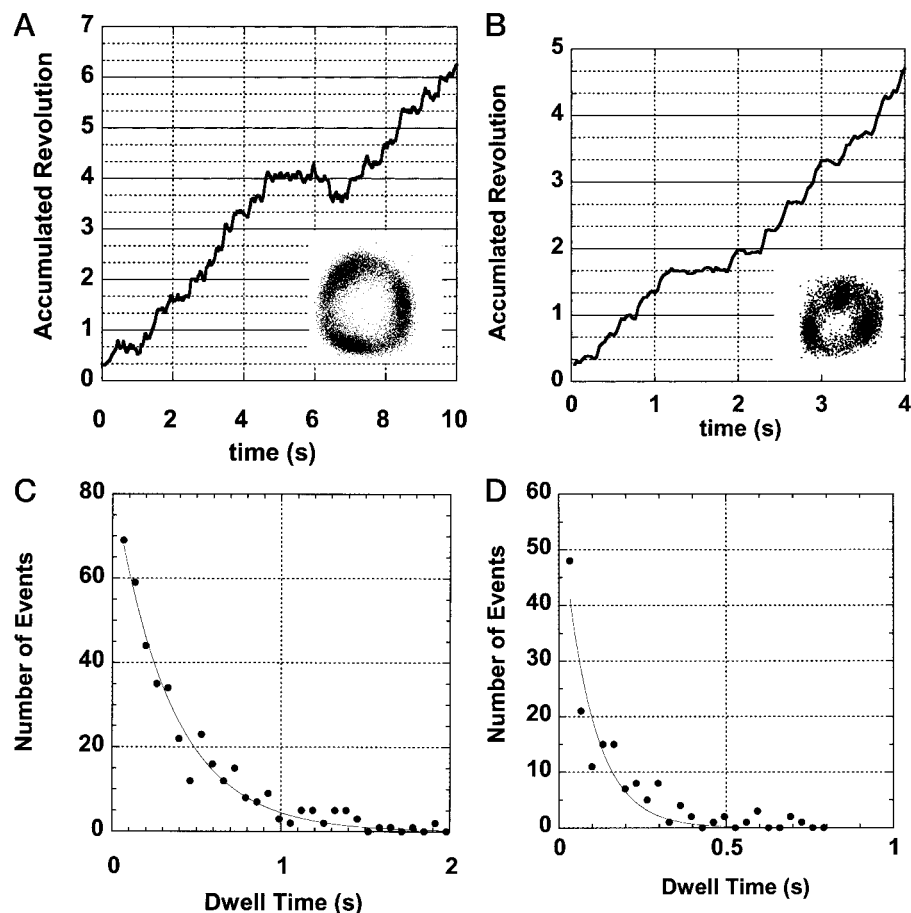


FIG. 3. **Comparison of the hydrolysis and rotational rates for different nucleotides.** *a*, time courses of hydrolysis monitored as NADH oxidation through the regeneration system. Blue, 2 mM ATP; green, 1 mM GTP; orange, 1 mM ITP; red, 3 mM UTP. Inset, enlarged view of the initial portion. The thick parts of the lines show the portion in which the hydrolysis rate shown in *c* was estimated. *b*, time courses of hydrolysis at lower nucleotide concentrations. Blue, 600 nM ATP; green, 3 μ M GTP; orange, 10 μ M ITP; red, 100 μ M UTP. *c*, comparison between hydrolysis and rotational rates. Closed circles, hydrolysis rates determined as in *a* and *b*. Open circles, rotational rates for 0.5–1.2- μ M actin filaments; 3 times the measured rates in revolutions s^{-1} are plotted for comparison with the hydrolysis rates. Error bars, S.D. Blue, ATP; green, GTP; orange, ITP; red, UTP. Rotational rates for ATP are from Ref. 10. Solid lines, except the one for ATP hydrolysis, show fit with $V = V_{\max}^a [NTP] / ([NTP] + K_m^a)$, where V_{\max}^a and K_m^a are 187 s^{-1} and 64 μ M for GTP hydrolysis, 157 s^{-1} and 202 μ M for ITP hydrolysis, 256.8 s^{-1} and 5.5 mM for UTP hydrolysis, 3.82 revolutions s^{-1} and 0.69 μ M for ATP-driven rotation, 3.28 revolutions s^{-1} and 3.43 μ M for GTP-driven rotation, and 3.95 revolutions s^{-1} and 13.3 μ M for ITP-driven rotation. The rates of ATP hydrolysis were fitted with $V = (V_{\max}^a K_m^b [NTP] + V_{\max}^b [NTP]^2) / ([NTP]^2 + K_m^b [NTP] + K_m^a K_m^b)$, where $V_{\max}^a = 87.5 s^{-1}$, $V_{\max}^b = 313 s^{-1}$, $K_m^a = 5.25 \mu$ M, and $K_m^b = 429 \mu$ M.

mixture (Fig. 3, *a* and *b*, insets).

The rate of ATP hydrolysis did not obey simple Michaelis-Menten kinetics and was fitted with two sets of K_m and V_{\max} : $V_{\max}^a = 87.5 s^{-1}$, $V_{\max}^b = 313 s^{-1}$, $K_m^a = 5.25 \mu$ M, and $K_m^b = 429 \mu$ M (Fig. 3*c*). The maximum rate of ATP hydrolysis, V_{\max}^b ,

FIG. 4. Stepping rotation at low nucleotide concentrations. *a* and *b*, time courses of rotation at $1 \mu\text{M}$ GTP (actin length $0.95 \mu\text{m}$) and at $10 \mu\text{M}$ ITP (actin length $1.01 \mu\text{m}$). *Insets*, traces of the centroid of the actin filament. *c* and *d*, histograms of the dwell times between steps. Rotation records in *a* and *b* were analyzed and are shown in *c* and *d*. *Lines* indicate an exponential fit: constant $\times \exp(-kt)$, where k is the rate for nucleotide binding (2.9 s^{-1} for $1 \mu\text{M}$ GTP and 11.1 s^{-1} for $10 \mu\text{M}$ ITP).



of 313 s^{-1} is higher than the previous value (10) of 177 s^{-1} , presumably because of the thorough removal of the bound nucleotide and aggregated enzyme. An additional factor is the increase of the amount of pyruvate kinase, which may limit the overall reaction rate, to 0.2 mg/ml , compared with 0.05 mg/ml in the previous study. The rates for GTP and ITP hydrolysis could be accounted for by simple Michaelis-Menten kinetics; V_{max} and K_m were 187 s^{-1} and $64 \mu\text{M}$, respectively, for GTP and 157 s^{-1} and $202 \mu\text{M}$ for ITP.

In contrast to the purine nucleotides, UTP hydrolysis activity gradually increased with time (Fig. 3, *a* and *b*). This cannot be ascribed to the slow response of the UTP-regenerating system, because it could generate UTP from UDP much faster (0.5 s^{-1}) than the acceleration (0.017 s^{-1} at 1 mM UTP). Slow binding of UTP to noncatalytic sites could explain the acceleration, but evidence is absent. Because the activation took a longer time at lower UTP concentrations, fully activated rate of UTP hydrolysis was estimated from the slope between 150 and 200 s at $>300 \mu\text{M}$, between 250 and 300 s at $100 \mu\text{M}$, and between 1000 and 1200 s at $30 \mu\text{M}$. As seen in Fig. 3c, hydrolysis of UTP was much slower than that of the purine nucleotides. To confirm that the measured hydrolysis rate was that of UTP and not of contaminants, we also measured P_i released in the medium. Although the rate of P_i release was around half the hydrolysis rate determined from NADH oxidation, presumably because of the absence of the UTP-regenerating system, TF_1 produced P_i equivalent to $>40\%$ of UTP in 5 min. Thus, TF_1 did hydrolyze UTP, not contaminating other nucleoside-triphosphates, which amounted to $<0.5\%$ (see "Experimental Procedures"). CTP, in contrast, was not hydrolyzed; the rate of P_i release at 2 mM CTP measured over 60 min was indistinguishable from the rate without the enzyme ($<0.01 \text{ s}^{-1}$).

As seen in Fig. 3c, the maximal hydrolysis rates for the four

nucleotides, ATP, GTP, ITP, and UTP, do not differ greatly. The major difference among the four is in the apparent K_m values, UTP being the highest. In this regard, it is possible that CTP is also hydrolyzed with a similar V_{max} but with a K_m far above 10 mM . Another difference is that ATP hydrolysis shows significant deviation from the simple Michaelis-Menten kinetics, which is not apparent for the other nucleotides. This may be correlated with the stronger tendency toward inhibition with ATP than with the other nucleotides (Fig. 3, *a* and *b*). The possibility that the other nucleotides also show deviation at much higher concentrations (giving possibly the same V_{max}) cannot be dismissed.

GTP- and ITP-driven Rotation—GTP and ITP supported the rotation of the γ subunit in TF_1 . The rotation, observed through the motion of a fluorescent actin filament attached to the γ subunit, was counterclockwise without exception, as in the case of ATP-driven rotation. Rotation assays at less than $10 \mu\text{M}$ GTP or $10 \mu\text{M}$ ITP were made on the enzyme directly attached to a coverslip that had been covalently modified with Ni^{2+} -NTA (13). Compared with the previous method (10) of attaching the enzyme on Ni^{2+} -NTA-coated beads, the direct attachment resulted in a higher percentage of finding rotating filaments at low nucleotide concentrations.

Because the F_1 motor has been shown to be a 120° stepper (10), we compare 3 times the rotational rate of a short actin filament (0.5 – $1.3 \mu\text{m}$) with the corresponding hydrolysis rate (Fig. 3). At low nucleotide concentrations ($[\text{ATP}] < 0.1 \mu\text{M}$, $[\text{GTP}] < 1 \mu\text{M}$, $[\text{ITP}] < 10 \mu\text{M}$) where nucleotide binding is rate-limiting, the two rates agreed with each other, indicating that three molecules of purine nucleotide, whether ATP, GTP, or ITP, drive a full turn. The agreement also shows that the rotation in the presence of GTP or ITP was not due to possible ATP contamination, which was far below 5%. At higher nucle-

otide concentrations, the rotational rate saturated around 4 revolutions s^{-1} . This is simply due to the hydrodynamic friction against the rotating actin filament (10). At low nucleotide concentrations, the rotation was resolved into discrete 120° steps (Fig. 4, *a* and *b*). The histograms of dwell times between steps were fitted with a single exponential decay with the rate of $2.9 s^{-1}$ for $1 \mu M$ GTP and $11.1 s^{-1}$ for $10 \mu M$ ITP (Fig. 4, *c* and *d*), implying that a first order reaction, binding of GTP (ITP), triggers each 120° step. These rate constants agree with the hydrolysis rates (Fig. 3*c*), confirming again that each 120° step is driven by the hydrolysis of one molecule of GTP or ITP.

As seen in Fig. 4*a*, back steps occurred occasionally in GTP-driven rotation. ITP-driven rotation also showed occasional back steps (data not shown). The velocity of back steps was as fast as the forward one and thus is unlikely to be of purely thermal origin (10). A stochastic mistake in the order of substrate binding or product release among the three catalytic sites could explain the back steps.

UTP Does Not Drive γ Rotation—With commercial UTP at 4 mM, we occasionally observed slow rotation (e.g. 1.4 revolutions s^{-1}). We suspected that this might have been due to contaminants, because ATP at a concentration as low as 300 nM, for example, could account for the observed speed. Indeed, even CTP, which the $\alpha_3\beta_3\gamma$ does not hydrolyze, produced rotation at 0.3 revolutions s^{-1} at 2 mM. We therefore purified UTP and CTP (see “Experimental Procedures”) and examined rotation at $300 \mu M$, the highest concentration available after the column purification. To avoid possible nucleotide contamination from other sources, we attached an aggregate of biotinylated polystyrene beads to the γ subunit in place of an actin filament and observed the beads in bright field in the absence of the oxygen scavenger system. No rotating beads were found in six assays with UTP in which 5543 beads only fluctuated around a fixed point. Observation in each assay continued for more than 30 min, much longer than the time needed to activate UTP hydrolysis at $300 \mu M$ (~ 5 min). Six assays with CTP also gave negative results.

If hydrolysis of each UTP molecule produces a 120° step as with purine nucleotides, the rotational rate is expected to be $4.4 s^{-1}$ at $300 \mu M$ UTP. We therefore carried out parallel assays with 600 nM ATP where the rotational rate would be $1.5 s^{-1}$. 40 rotating beads were found out of 4299 fluctuating beads (five assays). We also made an “unpredicted test” in which we observed beads without knowing the identity of the nucleotide. No rotation was found with $300 \mu M$ UTP, and rotating beads were readily found in the presence of 600 nM ATP. We conclude that UTP cannot support rotation of the γ subunit carrying a bead aggregate, at least not at the rate expected from the hydrolysis rate. One possibility is that UTP hydrolysis, unlike the hydrolysis of purine nucleotides, is completely decoupled from γ rotation, even at no load. The other possibility is that UTP, with a different base structure, cannot supply sufficient power to drive the beads through 120° ; in this case, the rate of UTP hydrolysis by the loaded TF_1 would also be very low.

Torque and Efficiency—To compare torque and energy conversion efficiency among three purine nucleotides, ATP, GTP, and ITP, that supported γ rotation, the rotational velocities of actin filaments attached to the γ subunit on Ni^{2+} -NTA coated-beads were examined. Fig. 5 shows time courses of rotation for actin filaments with length around $2 \mu m$ (Fig. 5*a*) and 3 – $4 \mu m$ (Fig. 5*b*). The average rotational velocity was determined for each curve over a portion containing at least five consecutive revolutions without noticeably unnatural intermissions (e.g. the last part of the *brown* curve in Fig. 5*b* was omitted). The results are summarized in Fig. 5*c*. Most data for GTP-driven (green) and ITP-driven rotation (orange) are on or below the

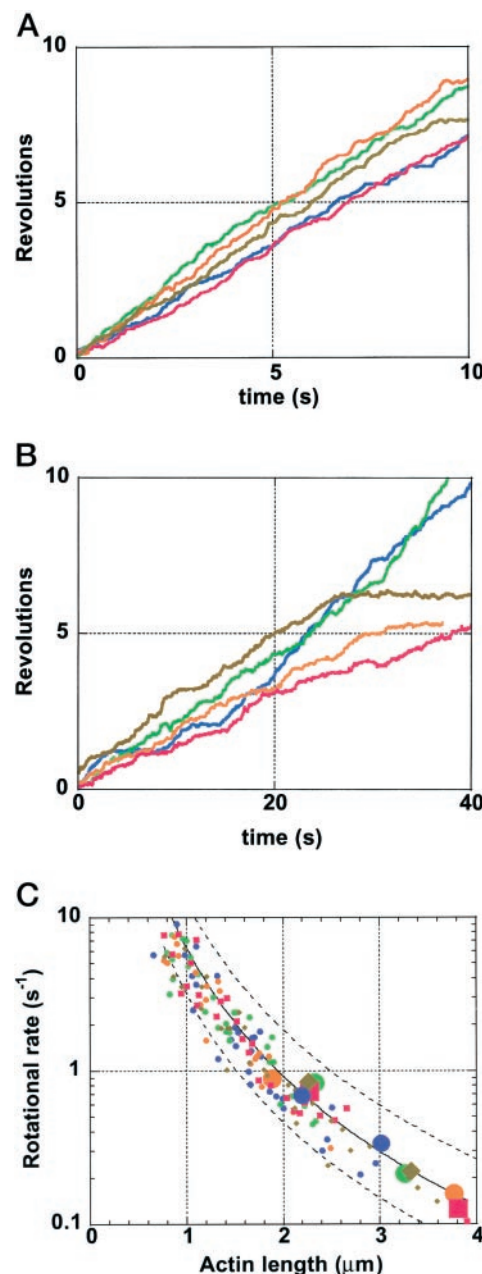


FIG. 5. Estimation of torque in GTP- and ITP-driven rotations. *a*, time courses of the rotation of an actin filament with length around $2 \mu m$. Blue, 2 mM ATP; green, 2 mM GTP; orange, 2 mM ITP; pink, 2 mM ATP, $10 \mu M$ ADP, and 100 mM P_i ; gold, 2 mM GTP, $10 \mu M$ GDP, and 100 mM P_i . *b*, time courses of the rotation with actin length of 3 – $4 \mu m$. See *a* for color coding. *c*, rotational rate versus the length of the actin filament. Blue circles, 2 mM Mg-ATP; green circles, 2 mM Mg-GTP; orange circles, 2 mM Mg-ITP; pink squares, 2 mM ATP, $10 \mu M$ ADP, and 100 mM P_i ($\Delta G_{ATP} = -80$ pN-nm/molecule); gold diamonds, 2 mM GTP, $10 \mu M$ GDP, and 100 mM P_i ($\Delta G_{GTP} = -80$ pN-nm/molecule). Large symbols indicate the data in *a* and *b*. Solid line, calculated rotational rate under an assumed constant torque of 40 pN-nm; dashed lines, constant torque at 80 and 20 pN-nm.

line representing the constant torque of 40 pN-nm, as is also the case for ATP-driven rotation (blue). We think that higher velocity values are more reliable, because any obstructions against rotation would reduce the velocity, and we conclude that TF_1 exerts a constant rotary torque of about 40 pN-nm regardless of the differences among the structures of purine rings. (The average torque calculated over all points in Fig. 5*c* is 32 ± 11 pN-nm for ATP, 35 ± 11 pN-nm for GTP, and 32 ± 10 pN-nm for ITP; these average values, however, are not

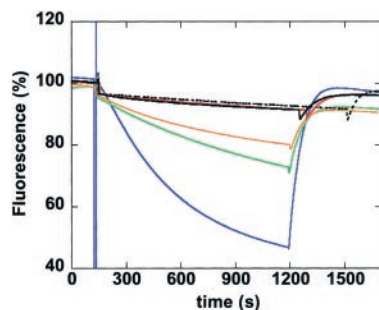


FIG. 6. **Proton pump activity of TF_0F_1 reconstituted into liposomes.** Translocation of protons into TF_0F_1 liposomes was monitored as the decrease in pyranine fluorescence. The reaction mixture contained 2 mM ATP (blue line), 2 mM GTP (green line), 2 mM ITP (orange line), 2 mM CTP (black line), 2 mM UTP (red line), or no nucleotide (dashed black line). The reaction was started by the addition of 4 mM $MgCl_2$. At 1200 s, 10 μ M FCCP was added to collapse the pH gradients.

meaningful, because the data in Fig. 5c have been selected for high torque values.)

The torque of 40 pN·nm times the angular displacement of $2\pi/3$ radians (equal to 120°), ~ 80 pN·nm, is the mechanical work done in a 120° step. In the previous study (10), it was shown that TF_1 does this much work even when the free energy available from ATP hydrolysis, ΔG_{ATP} , was reduced to -90 pN·nm/molecule. Here, we examined the torque and work in the presence of 2 mM ATP (or GTP), 10 μ M ADP (GDP), and 100 mM inorganic phosphate. Under these conditions, ΔG_{ATP} is calculated as -80 pN·nm/molecule from $\Delta G_{ATP} = \Delta G_0 + k_B T \ln[ADP][Pi]/[ATP]$, where $\Delta G_0 = -50$ pN·nm/molecule (17), $k_B T = 4.1$ pN·nm/molecule is thermal energy at room temperature, and ΔG_{GTP} should be of a similar value. As seen in Fig. 5c, the experimental points at $\Delta G_{ATP} = -80$ pN·nm/molecule (purple) and $\Delta G_{GTP} = -80$ pN·nm/molecule (brown) are indistinguishable from other points and also fall on or below the line for the constant torque of 40 pN·nm or constant work of 80 pN·nm (the torque averaged over plotted points is 35 ± 10 pN·nm for $\Delta G_{ATP} = -80$ and 32 ± 9 pN·nm for $\Delta G_{GTP} = -80$ pN·nm/molecule) This strengthens our contention that the efficiency of the energy conversion in this motor, from the hydrolysis (of purine nucleotides) into the mechanical work, can reach $\sim 100\%$.

Proton Pump—Nucleotide-driven proton uptake by the reconstituted TF_0F_1 liposome was measured, to see whether γ rotation is mechanically coupled to the proton pump. Liposomes were incubated with 2 mM nucleotide until the base line became stable, and then 4 mM $MgCl_2$ was added to start the reaction (Fig. 6). After 20 min, 10 μ M FCCP was added to collapse the pH gradients so as to ensure that the fluorescence decrease indicated the proton uptake. Fig. 6 clearly shows that the purine nucleotides ATP, GTP, and ITP drove the formation of pH gradient but UTP and CTP did not; the latter two gave signals that were indistinguishable from the control in the absence of a nucleotide. The initial rates of proton uptake by GTP and ITP in 1 min after starting the reaction were 30 and 27% of the ATP-driven uptake, respectively. The rate of nucleotide hydrolysis by TF_0F_1 , determined from the amount of inorganic phosphate released in 20 min, was 7.2 ± 1.4 s $^{-1}$ for ATP, 3.4 ± 0.5 s $^{-1}$ for GTP, and 2.7 ± 0.5 s $^{-1}$ for ITP. The three nucleotides show the same order in proton pumping and hydrolysis activities. The agreement suggests that GTP and ITP hydrolysis are coupled to proton pumping as efficiently as with ATP. Pyridine nucleotides were not good substrates for hydrolysis by TF_0F_1 ; the hydrolysis activity was not detected by the phosphate measurement (<0.12 s $^{-1}$ for 2 mM CTP and <0.09 s $^{-1}$ for 2 mM UTP).

DISCUSSION

In this paper, we have shown that the purine ring of a nucleotide is indispensable for γ rotation and for proton pumping in the F_0F_1 -ATPase. Both rotation and proton pumping were supported by the purine nucleotides, ATP, GTP, and ITP, but not by the pyrimidine nucleotides, CTP and UTP. Our results are consistent with the report by Perlin *et al.* (18), where GTP and ITP were shown to drive proton pumping in the F_0F_1 -ATPase, and support the idea that nucleotide hydrolysis is coupled to proton pumping through mechanical rotation of the γ subunit.

Our rotation assay has revealed that many of the rotational characteristics are common to all three purine nucleotides. (i) The rotary torque is constant around 40 pN·nm. (ii) The rotation consists of discrete 120° steps. (iii) Each 120° step is driven by the hydrolysis of one nucleotide molecule. (iv) Backward steps as fast as the forward ones occur occasionally. The first three points imply that the mechanical work done in a 120° step is about 80 pN·nm for all three nucleotides, and thus the energy conversion efficiency can reach $\sim 100\%$ with all three purine nucleotides. As to the last statement, we have shown in this study that the mechanical work of ~ 80 pN·nm is done even when ΔG_{ATP} or ΔG_{GTP} is reduced to -80 pN·nm/molecule. We did not ascertain a high efficiency in ITP-driven rotation, but Sorgato *et al.* (19) have reported that the energy from ITP hydrolysis is converted into a membrane potential by submitochondrial particles as efficiently as ATP hydrolysis. Thus, the efficiency of ITP-driven rotation is expected also to be close to 100%. The similarities among the three nucleotides suggest that the mechanical characteristics of the rotation such as the stepping, torque, and work per step are inherent in the (structure of the) F_1 motor. Purine nucleotides can trigger and let proceed the stepping mechanism in which the step angle, torque, and work are preset, whereas pyrimidine nucleotides cannot.

Chemical kinetics, in contrast, are different among the three purine nucleotides. First, the hydrolysis curves in Fig. 3c are shifted toward higher concentrations in the order of ATP, GTP, and ITP, and the rotation curves follow the same trend. Apparently, this is due to the difference in the rate of nucleotide binding, ATP being the fastest and ITP the slowest. Analysis of step intervals at low nucleotide concentrations supported this view; the rate constant was 2.5×10^7 M $^{-1}$ s $^{-1}$ for ATP (10), 2.9×10^6 M $^{-1}$ s $^{-1}$ for GTP, and 1.1×10^6 M $^{-1}$ s $^{-1}$ for ITP.

According to the binding change mechanism for ATP synthesis (1), much of the energy available from γ rotation during synthesis is used to release a tightly bound ATP into the medium. Conversely, during hydrolysis, binding of ATP powers the reverse rotation of γ . If the above difference in the rate constant of nucleotide binding reflects a similar difference in the affinity for the nucleotide, then the energy provided by ITP binding will be the smallest and might have been insufficient to power the stepping mechanism. Because all three purine nucleotides supported rotation, it seems either that the affinity for ITP is high enough (a 20-fold difference in the binding constant is equivalent to a free energy difference of only 12 pN·nm/molecule), or that the rate of nucleotide release decreases in the order of ATP to ITP and makes the affinities more or less the same. In this regard, it is possible that UTP, of which the hydrolysis curve in Fig. 3c is further shifted toward the right, cannot confer sufficient binding energy to the stepping mechanism.

A second difference in the chemical kinetics is that the ATP hydrolysis was described by two sets of K_m and V_{max} , whereas one set sufficed for GTP and ITP. The two sets for the case of ATP are usually ascribed to two modes of catalysis: bisite and

trisite, where one or two, or two or three, respectively, of the three catalytic sites are alternately filled with a nucleotide. The possibility, however, exists that the enzyme operates in the bisite mode at all concentrations at or above micromolar and that the apparent deviation from the simple Michaelis-Menten kinetics is due to the Mg-ADP inhibition. Single K_m values for the hydrolysis of GTP and ITP, which are shown to be less prone to inhibition, support this view, although two sets of K_m and V_{max} with similar V_{max}/K_m could also explain the simple kinetics. Resolution calls for the determination of the number of nucleotides bound in the catalytic sites of uninhibited enzyme, which is not an easy experiment.

The pyrimidine nucleotides, CTP and UTP, were poor substrates for the TF_1 and TF_0F_1 . CTP was not hydrolyzed and, naturally, did not drive γ rotation or proton pump. UTP was hydrolyzed by TF_1 , yet UTP did not support rotation and pumping. Ca-ATP has also been reported to be an uncoupling substrate for F_0F_1 , in that Ca-ATP was hydrolyzed without pumping protons (20). The kinetics of Ca-ATP hydrolysis, however, was similar to that of Mg-ATP hydrolysis. Thus, the nature of uncoupling seems different between the two cases, Ca-ATP and (Mg-)UTP. Interestingly, the reconstituted TF_0F_1 did not hydrolyze UTP, while TF_1 (the $\alpha_3\beta_3\gamma$ subcomplex) did. This finding is consistent with the report by Yokoyama *et al.* (21) that the substrate specificity of this enzyme is higher when it contains a fuller complement of subunits. The UTP hydrolysis activity of the $\alpha_3\beta_3\gamma$ subcomplex may be ascribed to some flexibility in and around the catalytic site that would be suppressed in F_0F_1 ; such hydrolysis may proceed without a major structural change of the β subunit and thus without rotation of the γ subunit.

Acknowledgments—We thank Y. Harada, T. Nishizaka, K. Adachi, T. Hisabori, and E. Muneyuki for technical assistance and helpful discussions and H. Umezawa for laboratory management.

REFERENCES

1. Boyer, P. D. (2000) *Biochim. Biophys. Acta* **1458**, 252–262
2. Matsui, T., and Yoshida, M. (1995) *Biochim. Biophys. Acta* **1231**, 139–146
3. Boyer, P. D., and Kohlbrenner, W. E. (1981) in *Energy Coupling in Photosynthesis* (Selman, B. R., and Selman-Reimer, S., eds) pp. 231–240, Elsevier, Amsterdam
4. Oosawa, F., and Hayashi, S. (1986) *Adv. Biophys.* **22**, 151–183
5. Abrahams, J. P., Leslie, A. G., Lutter, R., and Walker, J. E. (1994) *Nature* **370**, 621–628
6. Aggeler, R., Haughton, M. A., and Capaldi, R. A. (1995) *J. Biol. Chem.* **270**, 9185–9191
7. Duncan, T. M., Bulygin, V. V., Zhou, Y., Hutcheon, M. L., and Cross, R. L. (1995) *Proc. Natl. Acad. Sci. U. S. A.* **92**, 10964–10968
8. Sabbert, D., Engelbrecht, S., and Junge, W. (1996) *Nature* **381**, 623–625
9. Noji, H., Yasuda, R., Yoshida, M., and Kinoshita, K., Jr. (1997) *Nature* **386**, 299–302
10. Yasuda, R., Noji, H., Kinoshita, K., Jr., and Yoshida, M. (1998) *Cell* **93**, 1117–1124
11. Tsunoda, S. P., Muneyuki, E., Amano, T., Yoshida, M., and Noji, H. (1999) *J. Biol. Chem.* **274**, 5701–5706
12. Bald, D., Amano, T., Muneyuki, E., Pitard, B., Rigaud, J. L., Kruip, J., Hisabori, T., Yoshida, M., and Shibata, M. (1998) *J. Biol. Chem.* **273**, 865–870
13. Adachi, K., Yasuda, R., Noji, H., Itoh, H., Harada, Y., Yoshida, M., and Kinoshita, K., Jr. (2000) *Proc. Natl. Acad. Sci. U. S. A.* **97**, 7243–7247
14. Yasuda, R., Noji, H., Yoshida, M., Kinoshita, K., Jr., and Itoh, H. (2001) *Nature* **410**, 898–904
15. Jault, J. M., Matsui, T., Jault, F. M., Kaibara, C., Muneyuki, E., Yoshida, M., Kagawa, Y., and Allison, W. S. (1995) *Biochemistry* **34**, 16412–16418
16. Matsui, T., Muneyuki, E., Honda, M., Allison, W. S., Dou, C., and Yoshida, M. (1997) *J. Biol. Chem.* **272**, 8215–8221
17. Stryer, L. (1995) *Biochemistry*, 4th Ed., pp. 443–462, Freeman, New York
18. Perlin, D. S., Latchney, L. R., Wise, J. G., and Senior, A. E. (1984) *Biochemistry* **23**, 4998–5003
19. Sorgato, M. C., Galianzo, F., Valente, M., Cavallini, L., and Ferguson, S. J. (1982) *Biochim. Biophys. Acta* **681**, 319–322
20. Papageorgiou, S., Melandri, A. B., and Solaini, G. (1998) *J. Bioenerg. Biomembr.* **30**, 533–541
21. Yokoyama, K., Hisabori, T., and Yoshida, M. (1989) *J. Biol. Chem.* **264**, 21837–21841